ARTICLES

Vacuum Ultraviolet (VUV) Pulsed Field Ionization−Photoelectron and VUV−IR Photoinduced Rydberg Ionization Study of *trans*-Dichloroethene†

H. K. Woo, P. Wang, K. C. Lau, X. Xing, and C. Y. Ng*

Department of Chemistry, University of California at Davis, One Shields Avenue, Davis, California 95616

Received: March 25, 2004; In Final Form: June 17, 2004

The vacuum ultraviolet (VUV) pulsed field ionization−photoelectron (PFI−PE) spectrum for *trans*-dichloroethene (*trans*-ClCH═CHCl) has been measured in the energy range 77 600−79 200 cm^{-1}. On the basis of the spectral simulation of the origin VUV−PFI−PE vibrational band, we have determined the IE(*trans*-ClCH═CHCl) to be 77 678.4 ± 2.0 cm^{-1} (9.630 97 ± 0.000 25 eV). The vibrational bands resolved in the VUV−PFI−PE spectrum of *trans*-ClCH═CHCl are assigned on the basis of ab initio vibrational frequencies and calculated Franck−Condon factors for the ionization transitions, yielding eight vibrational frequencies $\nu_1^+ = 163$ cm^{-1}, $\nu_3^+ = 367$ cm^{-1}, $\nu_4^+ = 871$ cm^{-1}, $\nu_5^+ = 915$ cm^{-1}, $\nu_6^+ = 944$ cm^{-1}, $\nu_8^+ = 1235$ cm^{-1}, $\nu_9^+ = 1258$ cm^{-1}, $\nu_{10}^+ = 1452$ cm^{-1}. The distinct feature of the VUV−PFI−PE spectrum is the strong vibrational progression of the ν_3^+ (C−Cl stretching) mode of *trans*-ClCH═$CHCl^+$, which is consistent with the theoretical geometry calculation, predicting a significant change in the C−Cl bond distance upon photoionization of *trans*-ClCH═CHCl. We have also determined the frequency (3068 cm^{-1}) for the ν_{11}^+ (C−H stretching) vibrational mode of *trans*-ClCH═$CHCl^+$ by employing the VUV−IR-photoinduced Rydberg ionization (VUV−IR−PIRI) method. The VUV−IR−PIRI spectra for *trans*-ClCH═CHCl prepared in the effective principal quantum numbers, $n^* = 14$ and 36, are found to be identical, supporting the previous conclusion that the Rydberg electron behaves as a spectator; i.e., the Rydberg electron orbital is conserved during the IR excitation of the ion core.

I. Introduction

The developments of pulsed field ionization (PFI) techniques[1−6] and high-resolution VUV light sources[7−10] have had a profound impact on the spectroscopic, energetic, and reactivity studies of simple neutral and cationic molecular systems.[11−15] The PFI techniques include PFI−photoelectron (PFI−PE)[1,2,11,13] and PFI−photoion (PFI−PI)[3,4] detections for spectroscopic measurements, the PFI−PE−photoion coincidence (PFI−PEPICO)[11,12] method for unimolecular dissociation studies, and the PFI−PE-secondary ion coincidence scheme[14,15] for bimolecular ion−neutral reaction studies.

The PFI−PE and PFI−PEPICO schemes have made possible the determination of accurate thermochemical data for simple molecular systems,[11] such as ionization energies (IEs),[16] 0 K dissociative photoionization thresholds,[12] and 0 K bond dissociation energies,[17] with unprecedented precisions. Through appropriate thermochemical cycles, these PFI measurements can also be translated into precise 0 K heats of formation[18] for neutral and cationic species. Taking advantage of these abilities, we are undertaking a project to perform PFI−PE and PFI−PEPICO measurements of representative classes of molecular species, which contain a variety of chemical elements. The main goal of these measurements is to provide a precise energetic database for the further development of more accurate semiempirical quantum calculation procedures.[19,20] For Cl-containing species, we have focused on the PFI study of chlorinated ethenes.[21−23] Because chlorinated ethenes are known industrial pollutants,[24] the energetic measurements of these molecules are also of interest to environmental studies.[25] The previous He I photoelectron and photoionization efficiecncy (PIE) studies have yielded values of 9.63−9.69 eV for the ionization energy (IE) of *trans*-dichloroethene (*trans*-ClCH═CHCl).[26−28] This report presents the result of a PFI−PE study of (*trans*-ClCH═CHCl). As shown below, the IE(*trans*-ClCH═CHCl) obtained in the present PFI−PE study is significantly more precise than the previous measurements.

Currently, the PFI−PE method represents a state-of-the-art method for vibrational spectroscopy measurements of polyatomic ions.[29] For single-photon VUV photoionization studies, the Franck−Condon factors (FCFs) involved can be calculated by ab initio quantum chemical procedures.[30,31] Together with ab initio vibrational frequencies, the theoretical FCF spectrum has allowed the reliable assignments of most vibrational bands resolved in the VUV−PFI−PE spectra of many polyatomic molecules.[22,29,32] However, for two-photon UV PFI−PE studies, the nature of the intermediate vibronic state involved is often not known, making it difficult to perform a reliable FCF simulation. Consequently, the vibrational assignments of two-photon UV PF−PE spectra can be more complicated.

The single-photon VUV−PFI−PE method can be limited by negligible FCFs. Many ion vibrational modes cannot be excited

† Part of the special issue "Tomas Baer Festschrift".

* To whom correspondence should be addressed. E-mail: cyng@chem.ucdavis.edu.

10.1021/jp040250s CCC: $27.50
Published on Web 08/24/2004

by photoionization because the bonding properties between atoms associated with these vibrational modes are unaffected by ejection of the photoelectron. It has been shown that high-frequency vibrational modes involving C—H, O—H, and N—H stretches, which are indiscernible in VUV−PFI−PE measurements, can be observed by autoionization-detected infrared (IR) spectroscopy[33,34] and IR-photoinduced Rydberg ionization[35] (PIRI) studies. In these experiments, high-*n* Rydberg states were prepared by a ultraviolet 1+1 resonance-enhanced mechanism, which requires the existence of a long-lived, bound intermediate electronic state. We have recently demonstrated the first VUV−IR−PIRI study on trichloroethene and *trans*-2-butene by combining tunable VUV and IR lasers.[21] The fact that the VUV−IR−PIRI scheme does not require an intermediate state of the neutral species makes it a general scheme, applicable to all molecular species. The VUV−IR−PIRI scheme is complementary to the VUV−PFI−PE method for vibrational-frequency measurements of molecular ions. By first exciting the molecule to sufficiently high-*n* Rydberg states prior to the IR−PIRI measurements, we find that the VUV−IR−PIRI spectra are independent of *n*, where *n* is the principal quantum number.[21] This observation indicates that the Rydberg electron behaves as a spectator during the ion core excitation step, and that the VUV−IR−PIRI spectrum observed represents the IR spectrum of the ion. Thus, the assignment of vibrational bands resolved in the VUV−IR−PIRI spectrum can also be facilitated by ab initio quantum chemical calculations. The VUV−IR−PIRI scheme is employed in the present study to measure the C—H stretching frequency of *trans*-ClCH═CHCl$^+$, which cannot be examined in VUV−PFI−PE measurements.

II. Experiment

A. VUV−PIE and VUV−PFI−PE Measurements. The details of the VUV laser photoion−photoelectron apparatus used in this study have been described previously.[21,22,29,32] In this experiment, the VUV laser radiation is generated via nonlinear four-wave difference frequency mixings in a Kr gas cell. The gas cell is equipped with a fused silica entrance window and a MgF_2 exit window. The Kr pressure used in the gas cell is ≈80 Torr. The UV frequency ω_1 is fixed at 47 061.831 cm^{-1} (212.49 nm in air) to match the two-photon resonance of the Kr 4p → 5p transition at 94 093.66 cm^{-1}. This 212.49 nm light pulse is generated by frequency-doubling of the 425 nm output of a dye laser (Laser Analytical System, LDL 20505), which is pumped by the 355 nm output of an injection seeded Nd:YAG laser (Spectra-Physics, GCR-290) operated at 30 Hz. The visible frequency ω_2 in the range of 14 894−16 494 cm^{-1} (606−671 nm) is generated by the second dye laser (Laser Analytical System, LDL 20505) pumped with the 532 nm output of the same Nd:YAG laser. The UV and visible light pulses are merged via a dichroic mirror and focused (focal length = 30 cm) into the Kr gas cell. The resulting VUV ($2\omega_1 - \omega_2$) light is separated from the UV and visible fundamental lights via a windowless VUV monochromator (McPherson model 343). The monochromator also serves to focus the VUV light to the photoionization region. The VUV light intersects the sample beam in the photoionization region at 90°, where ions and electrons are produced. After passing through the photoionization region, the VUV beam is intercepted by a copper photoelectric detector for monitoring the VUV light intensities. During the experiment, the ω_2 output is continuously monitored by a wavemeter (Coherent WaveMaster) for the purpose of frequency calibration.

The *trans*-dichloroethene sample (98% purity) was purchased from Aldrich and used without further purification. The *trans*-dichloroethene gas sample was introduced into the photoionization region of the photoion−photoelectron apparatus in the form of a skimmed supersonic beam. The *trans*-dichloroethene sample container was maintained at 0 °C using an ice−water bath such that the vapor pressure for *trans*-dichloroethene is ≈100 Torr. The vapor of *trans*-dichloroethene was premixed with helium to a total stagnation pressure of 1.5 atm in the sample container prior to expansion through a pulsed valve (nozzle diameter = 0.5 mm, repetition rate = 30 Hz). The beam source chamber and the photoionization chamber were evacuated by a 10 in. water-cooled diffusion pump (nominal pumping speed = 5000 L/s) and two turbomolecular pumps (pumping speed = 600 L/s each) and were maintained at pressures of 10^{-5} and 10^{-7} Torr, respectively, during the experiment.

The electron TOF detector and the ion TOF detector are situated below and above the photoionization region with the electron and ion TOF axes perpendicular to the VUV and molecular beams. For PFI−PE measurements, a dc field of ≤0.2 V/cm is applied to the photoionization region for dispersing the prompt background electrons away from the electron multichannel plate (MCP) detector. After a delay of ≈3 μs with respect to the firing of the VUV laser, a PFI field of 0.3 V/cm (width =100 ns) is applied to the photoionization region for field ionization of high-*n* Rydberg molecules prepared by VUV excitation. This PFI field also serves to extract PFI−PEs toward the electron MCP detector. Previous experiments[22,29,32] indicate that the PFI−PE resolution achieved is ≈1 cm^{-1} (full width at half-maximum, fwhm). Under the PFI conditions described above, the Stark shift for PFI−PE measurements associated with our apparatus has been shown to be governed by the relation, $4.1\sqrt{F}$ cm^{-1}, where F is the amplitude of the PFI pulse in (V/cm).[29] The energy scales for all the PFI−PE spectra presented here have been corrected according to this relation. For PIE measurements, a dc field of 2 V/cm is applied to the photoionization region to extract the ions toward the ion TOF tube, which are subsequently detected by the ion MCP.

The timing sequence for opening of the pulsed valve, firing of the Nd:YAG laser, and applying the PFI field is controlled by two digital delay units (Stanford Research DG535). The signal from the electron (or ion) MCP is preamplified before feeding into a boxcar integrator (Stanford Research SR250). The signal from the VUV light detector is fed into another boxcar integrator. Both boxcar integrators are interfaced to a personal computer, which also controls the scanning of the dye lasers. The PIE and PFI−PE spectra presented here have been normalized by the corresponding VUV light intensities.

B. VUV−IR−PIRI Measurements. The IR laser system used is a commercial optical parametric oscillator/amplifier (OPO/OPA) (LaserVision Inc.) pumped by the 1064 nm output of an injection seeded Nd:YAG laser (Spectra Physics Model: LAB-170, 15 Hz, 550 mJ/pulse at 1064 nm). The OPO stage is designed with grazing incidence grating cavity, which reduces the bandwidth of the IR output to ≈0.2 cm^{-1} (fwhm). The signal output of the OPO stage (712−880 nm) is guided to an output port to be monitored by a wave-meter (Coherent WaveMaster) for wavelength calibration. The idler output (1.3−2.0 μm) is directed to the OPA stage for difference-frequency mixing with the 1064 nm pumped beam to generate tunable IR laser radiation in the range 2.1−5.0 μm. Typical power output at the 3 μm region is ≈5 mJ/pluse. The IR light is aligned counter-propagating with the VUV beam. Maximum overlapping between the VUV and IR beam is confirmed by setting the toroidal grating to zero order and the IR laser power is measured outside the entrance window of the four-wave mixing gas cell.

In VUV−IR−PIRI measurement,[21] the *trans*-ClCH=CHCl molecules in the form of a supersonic beam are first excited to high-*n* Rydberg states by the VUV laser at a fixed frequency. The IR photon is then introduced at a delay of 20−50 ns with respect to the VUV laser pulse. After a delay of 50 ns with respect to the IR excitation, a pulsed electric field of 30 V/cm (width = 6 μs) is applied to the PI/PEX region for ions extraction. The VUV−IR−PIRI spectrum for *trans*-ClCH=CHCl is obtained by plotting the IR−PIRI intensity for *trans*-ClCH=CHCl$^+$ as a function of the IR frequency.

III. Theoretical Calculations

To assign the VUV−PFI−PE spectra and to determine a precise IE value for *trans*-ClCH=CHCl, we have performed ab initio quantum chemical calculations of the IE for *trans*-ClCH=CHCl, the anharmonic vibrational frequencies and rotational constants for *trans*-ClCH=CHCl/*trans*-ClCH=CHCl$^+$, and the FCFs for the ionization transitions: *trans*-ClCH=CHCl → *trans*-ClCH=CHCl$^+$. The procedures for these calculations are briefly described below.

A. IE Calculations. The adiabatic IE(*trans*-ClCH=CHCl) was calculated with two theoretical procedures: the Gaussian-3X (G3X)[19] and the CCSD(T,Full)/CBS extrapolation methods. The G3X calculation was made with the Gaussian 03 (G03) package of programs.[36] The CCSD(T,Full)/CBS calculation involved the approximation to the Complete Basis Set (CBS) limit at the level of couple cluster with single and double excitations plus a quasi-perturbative Triple excitations [CCSD(T)]. Specifically, the geometry optimizations were calculated at the CCSD(T)/6-311G(2df,p) level of theory. On the basis of the optimized geometry, single point energy calculations were carried out at the CCSD(T)/aug-cc-pV(X+d)Z/aug-cc-pVXZ (X = T, Q, and 5; standard aug-cc-pVXZ basis sets[37] is used on H and C and aug-cc-pV(X+d)Z basis set[38] is used on Cl) level of theory. The CBS energies were then estimated by a mixed exponent/Gauassian function of the form[39]

$$E(\mathrm{X}) = E_{\mathrm{CBS}} + B\exp[-(X-1)] + C\exp[-(X-1)^2] \quad (1)$$

where X = 3, 4, and 5 for aug-cc-pVTZ, aug-cc-pVQZ, and aug-cc-pV5Z, respectively. The zero-point vibrational energy (E_{ZPVE}) corrections were taken to be the sum ($1/2\sum_{i=1}^{12}\omega_i$) of all anharmonic vibrational frequencies (ω_i) at the CCSD(T)/6-311G(2df,p) level (see below). The core-valence electrons correlation (1s electrons on C and 2s/2p electrons on Cl) contributions (E_{CV}) were obtained at the CCSD(T) level using aug-cc-pwCVTZ basis set.[40] The energy due to the scalar relativistic effect (E_{SR}) was computed at configuration interaction with the singles and doubles (CISD) level of theory using the aug-cc-pVQZ basis set. And it is taken as the sum of the mass-velocity and one-electron Darwin terms in Breit−Pauli Hamiltonian.[41] All CBS energy calculations and correlation contributions were performed using the MOLPRO 2002.6 program suit.[42] The individual energetic contributions to IE(*trans*-ClCH=CHCl) are listed in Table 1.

B. Vibrational Frequencies Calculations. To assist the assignment of vibrational bands observed, we carried out high-level vibrational frequency calculations with anharmonicity corrections. First, harmonic vibrational frequencies and anharmonic effects for *trans*-ClCH=CHCl/*trans*-ClCH=CHCl$^+$ were both calculated at the MP2/6-311G(2df,p) level of theory using the G03 package of programs. To obtain better harmonic vibrational frequencies, we further performed calculations at the CCSD(T)/6-311G(2df,p) level using the MOLPRO 2002.6 program. The CCSD(T) harmonic vibrational frequencies are then corrected with the anharmonicities obtained at the MP2/6-311G(2df,p) level to yield anharmonic vibrational frequencies effectively at the CCSD(T)/6-311G(2df,p) level of theory.

TABLE 1: Individual Energy Contributions to the Total Energy for *trans*-ClCH=CHCl and *trans*-ClCH=CHCl$^+$ [a]

	trans-ClCH=CHCl	*trans*-ClCH=CHCl$^+$
extrapolated CBS[b]	−996.81421	−996.46035
E_{ZPVE}[c]	0.03268	0.03302
E_{CV}[d]	−0.64442	−0.64409
E_{SR}[e]	−2.83629	−2.83659
$\Delta E_{\mathrm{extrapolated\ CBS}}$	9.629	
ΔE_{ZPVE}	0.009	
ΔE_{CV}	0.009	
ΔE_{SR}	−0.008	
CBS IE[f]	9.639	
G3X IE[g]	9.61	
IE(expt)[h]	9.63097 ± 0.00025	

[a] Total energies are given in hartees and energy differences (Δ) and IEs are in electronvolts. [b] Extrapolated from the frozen-core total energies using eq 1. [c] Taken as the sum ($^1/_2\sum_{i=1}^{12}\omega_i$) of all anharmonic vibrational frequencies at the CCSD(T)/6-311G(2df,p) level. [d] Core-valence electrons correlation obtained at the CCSD(T)/aug-cc-pwCVTZ level. [e] Scalar relativistic effect calculated at the ClSD/aug-cc-pVQZ level. [f] CBS IE = $\Delta E_{\mathrm{extrapolated\ CBS}} + \Delta E_{\mathrm{ZPVE}} + \Delta E_{\mathrm{CV}} + \Delta E_{\mathrm{SR}}$. [g] G3X IE calculated using the G3X procedures. [h] IE(expt) is the experimental IE obtained in the present study.

C. Franck−Condon Factor Calculations. The FCF simulations were carried out using the momoFCF program made available by the Iwata group.[30,31] The simulations take into account the Duschinsky effect and assume that the potential energy surfaces of both *trans*-ClCH=CHCl and *trans*-ClCH=CHCl$^+$ are harmonic.[30] Because the vibrational ground state for *trans*-ClCH=CHCl is of a_g symmetry, vibrational bands with good intensities observed in the PFI−PE spectrum for *trans*-ClCH=CHCl$^+$ are expected to be of a_g symmetry. We note that vibational bands not predicted by the FCF calculations can also occur by anharmonicity couplings and ionization mechanisms via intermediate autoionizing states. The MP2 optimized geometries, vibrational frequencies, and normal mode displacement vectors were used. Because of the weak intensities in the higher order overtones ($>5\nu^+$), we have limited the number of transitions involved in the simulations. The allowed vibrational transitions were from *trans*-ClCH=CHCl ($\nu_1 = 0$, $\nu_2 = 0$, ..., $\nu_{12} = 0$) → *trans*-ClCH=CHCl$^+$ ($\nu_1^+ = x_1$, $\nu_2^+ = x_2$, ..., $\nu_{12}^+ = x_{12}$), where individual x_i (i = 1−12) values could be any integer from 0 to 5.

D. Rotational Constants Calculations. We have also obtained rotational constants for *trans*-ClCH=CHCl and *trans*-ClCH=CHCl$^+$ at the CCSD(T)/6-311G(2df,p) level of theory. These constants are used in the simulation of rotational fine structures of the origin PFI−PE vibrational band of *trans*-ClCH=CHCl$^+$ as described below. Table 2 displays the calculated rotational constants and the corresponding geometrical parameters [bond lengths (r), bond angles ($\angle$)] for *trans*-ClCH=CHCl and *trans*-ClCH=CHCl$^+$. The changes [Δ(ion−neutral)] in bond lengths, bond angles, and rotational constants between *trans*-ClCH=CHCl$^+$ and *trans*-ClCH=CHCl are also given in Table 2.

IV. Results and Discussion

A. Simulation of the Origin VUV−PFI−PE Vibrational Band. Using the calculated rotational constants for *trans*-ClCH=CHCl and *trans*-ClCH=CHCl$^+$, we have performed a semiempirical simulation of the origin VUV−PFI−PE vibra-

TABLE 2: Calculated Rotational Constants (*A, B, C* and A^+, B^+, C^+), Bond Lengths (*r*), and Bond Angles (∠) for *trans*-ClCH=CHCl and *trans*-ClCH=CHCl$^+$ Obtained at the CCSD(T)/6-311G(2df,p) Level of Theory

	trans-ClCH=CHCl	*trans*-ClCH=CHCCl$^+$	Δ(ion−neutral)[a]
	Rotational Constants (cm^{-1})		
A/A^+	1.755	1.673	−0.082
B/B^+	0.050	0.053	0.003
C/C^+	0.049	0.051	0.002
	Bond Length (Å)		
r(C−Cl)	1.733	1.652	−0.081
r(C=C)	1.331	1.397	0.066
R(C−H)	1.083	1.089	0.006
	Bond Angles (deg)		
∠(C−C−Cl)	121.2	120.5	−0.7
∠(C−C−H)	123.8	121.9	−1.9

[a] Difference between *trans*-ClCH=CHCl$^+$ and ClCH=CHCl.

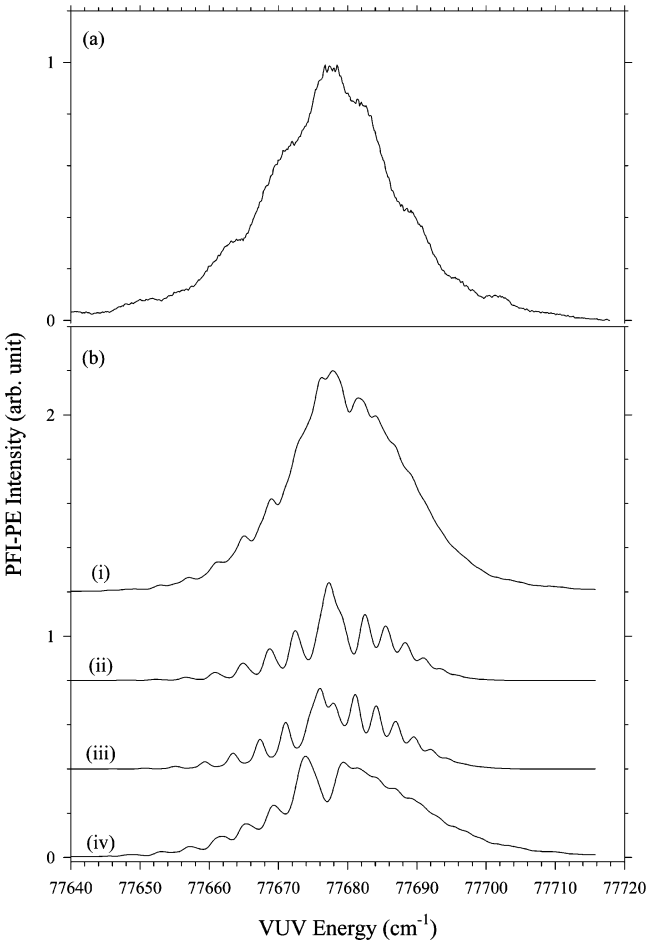

Figure 1. (a) Origin VUV−PFI−PE vibrational band for *trans*-ClCH=CHCl$^+$ in the energy range of 77 600−79 200 cm-^{1}. (b) Curve i: Simulated spectra for *trans*-ClCH=CHCl obtained by using a rotational temperature of 30 K and a Gaussian width of 1.5 cm^{-1} (fwhm). Curve ii: Contributions by the Q branches ($\Delta J = 0$, $\Delta K = 0, \pm 1$). Curve iii: Contributions by the P plus R branches ($\Delta J = \pm 1$, $\Delta K = 0, \pm 1$). Curve iv: Contributions by ($\Delta J = 0, \pm 1$; $\Delta K = \pm 2$) plus ($\Delta J = \pm 2$; $\Delta K = 0, \pm 1, \pm 2$).

tional band of *trans*-ClCH=CHCl$^+$ (Figure 1a), aiming to obtain a more precise value for the IE(*trans*-ClCH=CHCl). The detailed procedures for the simulation have been described previously.[43] The best simulation is achieved using a rotational temperature of 30 K for *trans*-ClCH=CHCl and a Gaussian instrumental line width of 1.5 cm^{-1} (fwhm). Curve i of Figure 1b depicts the overall simulation curve, which represents the sum of the contributions from the Q ($\Delta J = 0$, $\Delta K = 0, \pm 1$) (curve ii), P plus R ($\Delta J = \pm 1$, $\Delta K = 0, \pm 1$) (curve iii), and other ($\Delta J = 0, \pm 1$; $\Delta K = \pm 2$) plus ($\Delta J = \pm 2$; $\Delta K = 0, \pm 1, \pm 2$) (curve iv) rotational branches. The agreement between the origin VUV−PFI−PE band (Figure 1a) and the overall simulated spectrum (curve i of Figure 1b) is reasonably good except that the intensity of curve i on the high energy side is too high and that on the low energy side is too low compared to the experimental band of Figure 1a. We note that the semiempirical simulation scheme used here has not taken into account local perturbations by near resonance Rydberg states, it is not expected to yield correct intensities for individual rotational photoionization transitions. However, the simulation shows that the peak of the origin PFI−PE vibrational band is contributed by the Q-branch and thus can be used to determine the IE of *trans*-dichloroethene. Taking into account the Stark shift,[29] the IE(*trans*-ClCH=CHCl) is determined to be 77 678.4 ± 2.0 cm^{-1} (9.630 97 ± 0.000 25 eV) by the simulation.

The theoretical predictions for the IE(*trans*-ClCH=CHCl) are 9.61 eV by G3X and 9.639 eV by CCSD(T,Full)/CBS method (see Table 1). The experimental IE(*trans*-ClCH=CHCl) value of 9.630 97 ± 0.000 25 eV is in better agree with the IE calculated by the CCSD(T,Full)/CBS procedures. In recent studies,[22,29,32,44] we find that the CBS method generally yields better IE predictions than the G3X procedure. The discrepancies between the CBS IE predictions and experimental IE for polyatomic species based on PFI−PE measurements are <20 meV.

B. Comparison of the Origin PFI−PE Vibrational Band and the PIE Threshold. The threshold law for direct photoionization predicts a step function behavior for the PIE onset. Due to the hot band effect, photoions can be formed at energies below the true IE, giving rise to a tailing structure toward lower energies. In recent VUV−PIE and VUV−PFI−PE studies of *cis*-/*trans*-2-butenes,[29,32] *cis*-/*trans*-1-bromopropenes,[44] and trichloroethene,[22] we find that the IE value determined by the VUV−PFI−PE spectrum is in excellent agreement with the lowest energy at which the PIE reaches its plateau value, i.e., the top of the PIE step after correcting for the contribution from autoionization. This observation is consistent with the argument that all molecules, including the molecules in the ground state would ionize at the true IE. Because the PIE at a given energy measures the sum of all the photoion intensities, the PIE is expected to reach the top or plateau of the PIE step at the true IE value.

Figure 2 compares the PIE curve near the ionization onset with the origin VUV−PFI−PE vibrational band of *trans*-ClCH=CHCl$^+$. The dotted horizontal line shown in Figure 2 is an estimate of the plateau of the PIE step, i.e., the PIE contribution above the dotted line is attributed to autoionization. In accordance with the observation of previous studies, the lowest energy position of the PIE step (marked by an arrow in Figure 2) is in excellent agreement with the peak of the origin VUV−PFI−PE vbirational band, which is shown in the simulation to mark the IE(*trans*-ClCH=CHCl). Thus, the result of the present experiment is consistent with the previous conclusion that the lowest energy at which the PIE reaches its plateau value can be used to mark the true IE.[22,29,32,44]

C. FCF Simulation and Assignment of the VUV−PFI−PE Vibrational Bands. Figure 3 depicts the VUV−PFI−PE spectrum for *trans*-ClCH=CHCl in the VUV range of 77 600−79 200 cm^{-1} (upper energy scale), which corresponds to the frequency range of 0−1600 cm^{-1} measured with respect to the

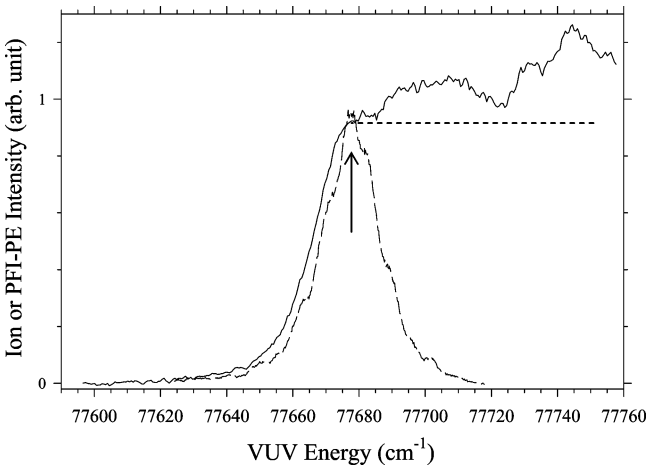

Figure 2. Comparison of the PFI−PE original band (dashed line) and PIE spectrum (solid line) for *trans*-ClCH═CHCl in the photon energy range of 77 600−77 760 cm^{-1}.

IE(*trans*-ClCH═CHCl). There are totally twelve vibrational modes for *trans*-ClCH═$CHCl^+$. On the basis of the calculated vibrational frequencies (see Table 3), 10 (ν_1^+ to ν_{10}^+) of the twelve vibrational frequencies are <1500 cm^{-1}. Thus, the scanning range of the present experiment would cover the excitation of ν_1^+ to ν_{10}^+ . Table 3 summaries the vibrational frequencies calculated at the MP2 and CCSD(T) levels for *trans*-ClCH═$CHCl^+$. The harmonic frequencies obtained via the MP2 and CCSD(T) methods are in general agreement with discrepancies <40 cm^{-1} except for the ν_7^+ mode where the discrepancies are ≈70 cm^{-1}.

Because the CCSD(T) frequencies are expected to be more accurate, the FCF spectrum shown in Figure 3b is obtained using the CCSD(T) frequencies. For the sake of comparison, the intensity of the origin vibrational band for the VUV−PFI−PE spectrum of Figure 3a and that for the calculated FCF spectrum of Figure 3b are arbitrarily normalized to unity. On the basis of the comparison of the frequencies measured with respect to the IE(*trans*-ClCH═CHCl) and relative intensities observed for

TABLE 3: Theoretical Vibrational Frequencies (cm^{-1}) for *trans*-ClCH═$CHCl^+$ Obtained Using the MP2/6-311G(2df,p) and CCSD(T)/6-311G(2df,p) Levels of Theory[a]

	MP2/6-311G(2df,p)			CCSD(T)/6-311G(2df,p)		
	H	AH	S	H	AH (MP2)	expt[b]
ν_1^+ (a_u)	170	169	165	166	164	163
ν_2^+ (b_u)	252	253	244	252	253	
ν_3^+ (a_g)	375	376	365	364	364	367
ν_4^+ (a_u)	880	861	855	867	848	871
ν_5^+ (b_g)	909	899	884	893	882	915
ν_6^+ (a_g)	989	975	961	952	939	944
ν_7^+ (b_u)	1031	1016	1002	961	946	
ν_8^+ (b_u)	1280	1257	1244	1268	1245	1235
ν_9^+ (a_g)	1294	1281	1258	1289	1276	1258
ν_{10}^+ (a_g)	1497	1459	1455	1491	1454	1452
ν_{11}^+ (b_u)	3211	3085	3121	3182	3058	3068
ν_{12}^+ (a_g)	3211	3088	3121	3185	3062	

[a] Abbreviations: H, harmonic Frequency; AH, anharmonic frequency; S, scaled frequency (scaling factor: 0.972). The AHs at CCSD(T)/6-311G(2df,p) are obtained by $AH(CCSD(T))_{MP2} = H(CCSD(T)/6\text{-}311G(2df,p) \times AH(MP2/6\text{-}311G(2df,p))/H(MP2/6\text{-}311G(2df,p)$. [b] Experimental values. This work.

the VUV−PFI−PE vibrational bands and the predicted frequencies and relative FCFs, we have assigned the VUV−PFI−PE bands (see Table 4). Generally, the FCF spectrum reproduces the experimental spectrum well. However, there are several peaks observed in the VUV−PFI−PE spectrum are not predicted by the FCF calculations. A more detailed analysis of the assignment is given below.

For *trans*-ClCH═CHCl, the neutral ground state is of a_g symmetry. As such, the FCF calculation predicts that the favorable vibrational transitions involve vibrational states of *trans*-ClCH═$CHCl^+$ with a_g symmetry. By comparing the FCF simulation with the experimental spectrum, several high-intensity peaks can be assigned with confidence. The first one is the peak at 367 cm^{-1}, which is assigned as ν_3^+ (a_g). Similar arguments apply to the peaks at 735, 946, 1106, 1261, 1311, and 1452 cm^{-1}, which are assigned as $2\nu_3^+$ (a_g), ν_6^+ (a_g), $3\nu_3^+$ (a_g), ν_9^+ (a_g), ($\nu_3^+ + \nu_6^+$) (a_g), and ν_{10}^+ (a_g), respectively. The FCF calculation also predicts $4\nu_3^+$ (a_g) at 1464 cm^{-1} (experi-

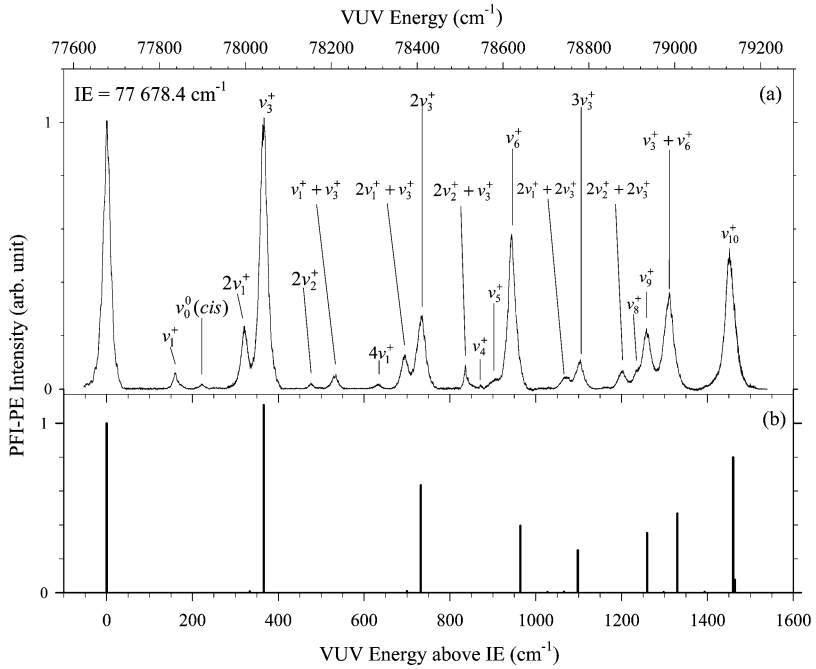

Figure 3. (a) VUV−PFI−PE spectrum of *trans*-ClCH═CHCl at energies up to 1600 cm^{-1} above the IE(*trans*-ClCH═CHCl). (b) Corresponding FCF simulation spectrum. The original bands for both the VUV−PFI−PE and FCF spectra are arbitrarily normalized to unity.

TABLE 4: Assignments of the Vibrational Bands Resolved in the VUV−PFI−PE Spectrum for *trans*-ClCH=CHCl$^+$ Based on FCF Calculations and Theoretical Vibrational Frequencies

	VUV−PFI−PE[a]		FCF calculation[b]	
assignment (symmetry)	frequencies (cm^{-1})	relative intensities	CCSD(T)/MP2[c] frequencies (cm^{-1})	relative[d] FCFs
ν_1^+ (a_u)	163	0.0604	164/169	
ν_{00} (cis)[e]	221	0.0191		
$2\nu_1^+$ (a_g)	322	0.2356	328/338	0.0087
ν_3^+ (a_g)	367	1.0169	364/376	1.1142
$2\nu_2^+$ (a_g)	476	0.0232	506/506	0.0003
$\nu_1^+ + \nu_3^+$ (a_u)	534	0.0553	528/545	
$4\nu_1^+$ (a_g)	635	0.0196	656/676	0.0001
$2\nu_1^+ + \nu_3^+$ (a_g)	697	0.1284	692/714	0.0097
$2\nu_3^+$ (a_g)	735	0.2770	728/752	0.6444
$2\nu_2^+ + \nu_3^+$ (a_g)	836	0.0899	867/882	0.0004
ν_4^+ (a_u)	871	0.0163	848/861	
ν_5^+ (b_g)	915	0.0412	882/899	
ν_6^+ (a_g)	944	0.5808	939/975	0.4144
$4\nu_1^+ + \nu_3^+$ (a_g)	(1002)		1020/1052	0.0001
$2\nu_1^+ + 2\nu_3^+$ (a_g)	1072	0.0451	1056/1090	0.0056
$3\nu_3^+$ (a_g)	1104	0.1097	1092/1128	0.2574
$2\nu_2^+ + 2\nu_3^+$ (a_g)	1203	0.0698	1234/1258	0.0002
ν_8^+ (b_u)	1235	0.0724	1245/1280	
$\nu_2^+ + \nu_7^+$ (a_g)			1199/1269	0.0008
ν_9^+ (a_g)	1258	0.2278	1267/1259	0.3709
$\nu_3^+ + \nu_6^+$ (a_g)	1311	0.3632	1303/1351	0.4941
$3\nu_1^+ + \nu_4^+$ (a_g)	(1354)		1340/1368	0.0001
$\nu_1^+ + \nu_3^+ + \nu_4^+$ (a_g)	(1399)		1376/1406	0.0050
$2\nu_1^+ + 3\nu_3^+$ (a_g)	(1426)		1420/1466	0.0022
$2\nu_2^+ + \nu_6^+$ (a_g)	(1420)		1445/1481	0.0001
ν_{10}^+ (a_g)	1452	0.5272	1454/1459	0.7881
$4\nu_3^+$ (a_g)	(1468)		1456/1504	0.0798

[a] Experimental frequencies and relative intensities for vibrational bands observed in the VUV−PFI−PE spectrum for *trans*-ClCH=CHCl$^+$. The intensity for the origin PFI−PE vibrational band is arbitrarily normalized to 1.000. [b] FCF calculations using the MOMOFCF program [c] Theoretical vibrational frequencies are taken from Table 3. [d] The FCF for the origin vibrational band is arbitrarily normalized to 1.000. [e] Impurty band due to impurity of *cis*-dichloroethene.

mental prediction = 1468 cm^{-1}). However, because the intensity of the ν_{10}^+ (a_g) band is predicted to be 10 times stronger than that of the $4\nu_3^+$ (a_g) band, the $4\nu_3^+$ (a_g) band is most likely obscured by the ν_{10}^+ (a_g) band. Although the observed intensities for the VUV−PFI−PE bands are higher than those predicted by the FCF calculation, we have assigned the smaller peaks observed at 322, 476, 635, 697, 836, 1072, and 1203 cm^{-1} as $2\nu_1^+(a_g)$, $2\nu_2^+(a_g)$, $4\nu_1^+(a_g)$, $2\nu_1^+ + \nu_3^+(a_g)$, $2\nu_2^+ + \nu_3^+(a_g)$, $2\nu_1^+ + 2\nu_3^+(a_g)$, and $2\nu_2^+ + 2\nu_3^+(a_g)$, respectively.

For the rest of the observed peaks, although not predicted by the FCF calculation, assignments can be made on the basis of predictions of the theoretical frequencies. The first peak observed at 161 cm^{-1} is not predicted by the FCF simulation. The MP2/CCSD(T) calculations suggest that this peak arises from excitation of the ν_1^+ (a_u) mode. The PFI−PE peak at 221 cm^{-1} does not match any calculated frequencies. The comparison of the VUV−PFI−PE spectra of *trans*- and *cis*-dichloroethenes[23] shows that the position of this PFI−PE peak coincides with the origin PFI−PE vibrational band of *cis*-ClCH=CHCl [ν_0^0(cis)]. Thus, this peak is attributed to the impurity of *cis*-ClCH=CHCl in the gas sample. The intensity of this band is ≈0.02 relative to the origin PFI−PE vibrational band of *trans*-ClCHl=CHCl$^+$. This is consistent with the purity of 98% for the *trans*-dichloroethene sample specified by Aldrich. The next three unpredicted PFI−PE peaks are observed at 534, 871, and 915 cm^{-1}. The PFI−PE peak at 534 cm^{-1} is consistent with the predicted frequency of 537 cm^{-1} for the ($\nu_1^+ + \nu_3^+$) (a_u) combination mode. The PFI−PE bands observed at 871 and 915 cm^{-1} are assigned as ν_4^+ (a_u) and ν_5^+ (b_u), respectively. The small shoulder observed at 1235 cm^{-1} is assigned as ν_8^+ (b_u). We note that the observations of vibrational bands with a_u and b_u symmetry are possible via intermediate autoionization states. Several vibrational bands predicted by the FCF calculation with relative intensities ≤0.005 (see Table 4) are not observed in the PFI−PE spectrum. The frequencies in parentheses for overtones and combination bands (see column 2 of Table 4) are values based on the experimental harmonic frequencies.

D. Vibrational Progression. A major feature of the VUV−PFI−PE spectrum of *trans*-ClCH=CHCl is the observation of the strong vibrational progressions of the ν_3^+ (a_g) mode. Combination bands involving ν_3^+ and its progressions are also distinctly observed, indicating that the equilibrium geometry of *trans*-ClCH=ClCH$^+$ in the ground state is distorted from that of *trans*-ClCH=ClCH along the ν_3^+ vibrational coordinates. As shown in Table 2, the differences in bond distances *r*(C−Cl) and r(C=C) between the ion and neutral [Δ(ion−neutral)] are significantly larger than those for r(C−H), suggesting that the C−Cl and C−C stretching modes for *trans*-ClCH=CHCl$^+$ are preferentially excited upon photoionization of *trans*-ClCH=CHCl. The change in *r*(C−Cl) is indicative of interaction between the lone pair electrons of Cl atoms and the π-electrons of the C=C bond. Because the ν_3^+ mode corresponds mainly to the C−Cl symmetric stretch vibration, the prediction of a significant change in *r*(C−Cl) can be taken as the rationalization for excitation of the ν_3^+ vibrational progression in the VUV−PFI−PE spectrum.

The theoretical frequency calculation shows that *trans*-ClCH=CHCl$^+$ has two C−H stretching modes, ν_{11}^+ (b_u) and ν_{12}^+ (a_g) with nearly identical frequencies of >3000 cm^{-1}. The ν_{12}^+ (a_g) mode is allowed for single-photon VUV photoionization; but its FCF intensity is predicted extremely small (<0.0001 relative to that of the origin PFI−PE vibrational band). The lack of excitation of the ν_{12}^+ (a_g) mode can be accounted for by the small change in *r*(C−H) upon VUV photoionization. For this reason, we have not performed PFI−PE measurements at frequencies >1600 cm^{-1} above the IE(*trans*-ClCH=CHCl).

E. VUV−IR−PIRI. Of the two C−H stretching modes, ν_{11}^+ (b_u) and ν_{12}^+ (a_g), only the ν_{11}^+ (b_u) mode is IR-active. Thus, we expected that the ν_{11}^+ (b_u) frequency can be measured by the VUV−IR−PIRI measurement. The VUV−IR−PIRI spectra for *trans*-ClCH=CHCl$^+$ in the IR region of 3010−3144 cm^{-1} are displayed in Figure 4. The two IR−PIRI spectra, plotted as curves i and ii in Figure 4 are obtained by setting the VUV frequency fixed at 77 134.8 and 77 596.6 cm^{-1}, respectively. Knowing the IE(*trans*-ClCH=CHCl) value from VUV−PFI−PE, the corresponding effective principal quantum number values, $n^* = 14$ and 36, for the Rydberg states excited in curves i and ii are marked in Figure 4. Two relatively low n^* values ($n^* = 14$ and 36) are chosen because we find that better signal-to-noise (S/N) ratios for the spectrum can be obtained with lower n^* values.[21] Although the n^* values are quite different, a single peak is resolved in both spectra at the same position centered at 3068 cm^{-1}. The latter VUV−IR−PIRI peak is assigned to excitation of the ν_{11}^+ (b_u) vibrational mode of *trans*-ClCH=CHCl$^+$. Similar observations, showing that the IR−PIRI spectrum is independent of n^* have been reported previously for VUV−IR−PIRI studies of *trans*-$CH_3CH{=}CHCH_3$ and $ClCH{=}CCl_2$.[21]

It is plausible that the IR−PIRI process observed in the present study follows a vibrational autoionization mechanism,[45] resulting in the formation of ions in the vibrational ground state.

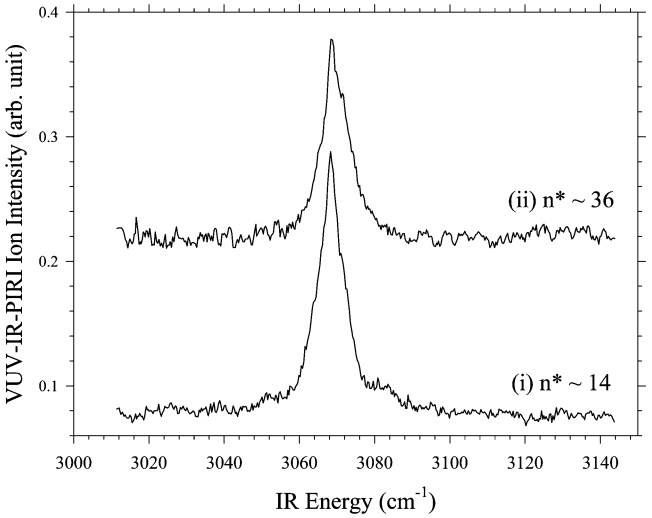

Figure 4. VUV−IR−PIRI spectra of *trans*-ClCH═CHCl in the region of 3010−3150 cm^{-1}. Curve i: VUV energy fixed at 77 134.8 cm^{-1}. Curve ii: VUV energy fixed at 77 596.6 cm^{-1}.

The measurement of the electron kintic energy distribution of the IR−PIRI process should reveal the nature of the autoionization mechanism. The independence of n^* observed for the IR−PIRI spectrum suggests that the electron Rydberg orbital is conserved, i.e., the Rydberg electron behaves as a spectator during the IR-excitation of the ion core.

Combining the VUV−PFI−PE and VUV−IR−PIRI measurements, we have determined nine of the twelve vibrational frequencies for *trans*-ClCH═$CHCl^+$. The experimental frequencies are compared to the theoretical MP2/CCSD(T) frequencies in Table 2. As expected, the CCSD(T) frequencies are generally in better agreement with the experimental frequencies.

Theoretical calculations at the MP2/6-311G(2df,p) level predict that the harmonic vibrational frequencies for *trans*-dichloroethene molecular ions with different isotopic distributions are essentially identical except four harmonic frequencies (ν_2^+, ν_3^+, ν_6^+, and ν_7^+) associated with C−Cl stretching and bending motions. For these vibrational modes, the harmonic frequencies for *trans*-^{35}ClCH═$CH^{35}Cl^+$ are higher by 1−4 cm^{-1} compared to the corresponding harmonic frequencies for trans-^{35}ClCH═$CH^{37}Cl^+$, which in turn are higher than those for *trans*-^{37}ClCH═$CH^{37}Cl^+$ by 1−4 cm^{-1}. Considering the fact that the ratio for the natural abundance of ^{35}Cl to that of ^{37}Cl is 0.76/0.24, we calculate the relative abundances for *trans*-^{35}ClCH═CH^{35}Cl, *trans*-^{35}ClCH═CH^{37}Cl, and *trans*-^{37}ClCH═CH^{37}Cl as 0.58:0.36:0.06, respectively. Due to the relatively small abundances for *trans*-^{35}ClCH═CH^{37}Cl and *trans*-^{37}ClCH═CH^{37}Cl, the vibrational bands observed in the PFI−PE measurement should be dominated by photoionization of *trans*-^{35}ClCH═CH^{35}Cl. That is, the vibrational frequencies determined in the present experiment can mostly be assigned to the vibrational modes of *trans*-^{35}ClCH═$CH^{35}Cl^+$.

V. Conclusions

The VUV−PFI−PE spectrum of *trans*-ClCH═CHCl has been obtained near its ionization threshold. On the basis of a semiempirical simulation of the origin PFI−PE vibrational band, the IE(*trans*-ClCH═CHCl) is determined to be 77 678.4 ± 2.0 cm^{-1} (9.630 97 ± 0.000 25 eV). The vibrational bands resolved in the VUV−PFI−PE spectra are assigned with the aid of calculated FCFs for the ionization transitions. A strong vibrational progression of the ν_3^+ mode is observed in the VUV−PFI−PE spectrum, which is rationalized by the predicted change in the r(C−Cl) distance upon photoionization. The VUV−IR−PIRI spectrum for *trans*-ClCH═$CHCl^+$ has also been measured to probe the ν_{11}^+ (b_u) C−H stretching frequency for *trans*-ClCH═$CHCl^+$. The observation that the VUV−IR−PIRI spectrum for *trans*-ClCH═$CHCl^+$ is independent of n^* is in accord with the results of previous studies on trichloroethene and *trans*-2-butene.

Acknowledgment. This work was supported by the U.S. Department of Energy, Office of Basic Energy Sciences, Division of Chemical Sciences, Geosciences, and Biosciences under Contract No. DE-FG02-02ER15306. The calculations of this work used resources of the National Energy Research Scientific Computing Center, which is supported by the Office of Science of the U.S. Department of Energy under Contract No. DE-AC03-76SF00098. Part of the calculations were also performed using the Molecular Science Computing Facility in the William R. Wiley Environmental Molecular Sciences Laboratory, a national scientific user facility sponsored by the U.S. Department of Energy's Office of Biological and Environmental Research and located at the Pacific Northwest National Laboratory. C.Y.N. also acknowledges partial supports by the AFOSR Grant No. F49620-03-1-0116 and NSF ATM 0317422.

References and Notes

(1) Schlag, E. W. *ZEKE Spectroscopy*; Cambridge University Press: Cambridge, U.K., 1996.
(2) Müller-Dethlefs, K.; Sanders, M.; Schlag, E. W. *Chem. Phys. Lett.* **1984**, *112*, 291.
(3) Zhu, L.; Johnson, P. M. *J. Chem. Phys.* **1991**, *94*, 5769.
(4) Johnson, P. M. *Adv. Ser. Phys. Chem. A* **1999**, *10*, 296.
(5) Hsu, C.-W.; Evans, M.; Ng, C. Y.; Heimann, P. *Rev. Sci. Instrum.* **1997**, *68*, 1694.
(6) Jarvis, G. K.; Song, Y.; Ng, C. Y. *Rev. Sci. Instrum.* **1999**, *70*, 2615.
(7) Kung, A. H.; Lee, Y. T. In *Vacuum Ultraviolet Photoionization and Photodissociation of Molecules and Clusters*; Ng, C. Y., Ed.; World Scientific: Singapore, 1991.
(8) Hepburn, J. W. *Laser Techniques in Chemistry*; Meyers, A., Rizzo, T. R., Eds.; Wiley: New York, 1994.
(9) Heimann, P.; Koike, M.; Hsu, C.-W.; Evans, M.; Lu, K. T.; Ng, C. Y.; Suits, A.; Lee, Y. T. *Rev. Sci. Instrum.* **1997**, *68*, 1945.
(10) Hollenstein, U.; Palm, H.; Merkt, F. *Rev. Sci. Instrum.* **2000**, *71*, 4023.
(11) Ng, C. Y. *Annu. Rev. Phys. Chem.* **2002**, *54*, 101.
(12) Jarvis, G. K.; Weitzel, K.-M.; Malow, M.; Baer, T.; Song, Y.; Ng, C. Y. *Rev. Sci. Instrum.* **1999**, *70*, 3892.
(13) Hollenstein, U.; Seiler, R.; Schmutz, H.; Andrist, M.; Merkt, F. *J. Chem. Phys.* **2001**, *115*, 5461.
(14) Qian, X.-M.; Zhang, T.; Chang, C.; Wang, P.; Ng, C. Y.; Chiu, Y.-H.; Levandier, D. J.; Miller, J. S.; Dressler, R. A.; Baer, T.; Peterka, D. S. *Rev. Sci. Instrum.* **2003**, *74*, 4096.
(15) Qian, X.-M.; Zhang, T.; Tang, X. N.; Ng, C. Y.; Chiu, Y.; Levandier, D. J.; Miller, J. S.; Dressler, R. A. *J. Chem. Phys.* **2003**, *119*, 10175.
(16) A list of IE of molecules and radicals determined by PFI−PE and PFI−PI measurements can be found at the ZEKE website (http://www.zeke.org/ie.html).
(17) Ng, C. Y. *J. Electron Spectrosc. Relat. Phenom.* **2000**, *112*, 31.
(18) Song, Y.; Qian, X.-M.; Lau, K.-C.; Ng, C. Y.; Liu, J.; Chen, W. *J. Chem. Phys.* **2001**, *115*, 4095.
(19) Curtiss, L. A.; Redfern, P. C.; Raghavachari, K.; Pople, J. A. *J. Chem. Phys.* **2001**, *114*, 108.
(20) Hu, L. H.; Wang, X. J.; Wong, L. H.; Chen, G. H. *J. Chem. Phys.* **2003**, *119*, 11501.
(21) Woo, H. K.; Wang, P.; Lau, K. C.; Xing, X.; Ng, C. Y. *J. Chem. Phys.* **2004**, *120*, 1756.
(22) Woo, H. K.; Lau, K.-C.; Ng, C. Y. *Chinese J. Chem. Phys.*, in press.
(23) Woo, H. K.; Wang, P.; Lau, K. C.; Xing, X.; Ng, C. Y. Unpublished results.
(24) Reiser, C.; Lussier, F. M.; Jensen, C. C.; Steinfeld, J. I. *J. Am. Chem. Soc.* **1979**, *101*, 350.

(25) Sato, K.; Tsunashima, S.; Takayanagi, T.; Fujisawa, G.; Yokoyama, A. *J. Chem. Phys*. **1997**, *106*, 10123.

(26) Watanabe, K.; Nakayama, T.; Mottl, J. *J. Quant. Spectrosc. Radiat. Transfer* **1962**, *2*, 369.

(27) Lake, R. F.; Thompson, H. *Proc. R. Soc. (London)* **1970**, *A315*, 323.

(28) Jonathan, N.; Ross, K.; Tomlinson, V. *Int. J. Mass Spectrom. Ion Phys.* **1970**, *4*, 51.

(29) Woo, H. K.; Lau, K.-C.; Zhan, J.-P.; Ng, C. Y.; Cheung, Y.-S.; Li, W. K.; Johnson, P. M. *J. Chem. Phys*. **2003**, *119*, 7789.

(30) Yamaguchi, M.; Momose, T.; Shida, T. *J. Chem. Phys.* **1990**, *93*, 4211.

(31) MomoFCF program can be obtained from http://hera.ims.ac.jp.

(32) Woo, H. K.; Zhan, J.; Lau, K.-C.; Ng, C. Y.; Cheung, Y.-S. *J. Chem. Phys.* **2002**, *116*, 8803.

(33) Fujii, A.; Iwasaki, A.; Ebata, T.; Mikami, N. *J. Phys. Chem. A* **1997**, *101*, 5963.

(34) Ebata, T.; Fujii, A.; Mikami, N. *Int. Rev. Phys. Chem.* **1998**, *331* and references therein.

(35) Gerhards, M.; Schiwek, M.; Unterberg, C.; Kleinermanns, K. *Chem. Phys. Lett.* **1998**, *297*, 515.

(36) Frisch, M. J.; Trucks, G. W.; Schlegel, H. B.; Scuseria, G. E.; Robb, M. A.; Cheeseman, J. R.; Montgomery, J. A., Jr.; Vreven, T.; Kudin, K. N.; Burant, J. C.; Millam, J. M.; Iyengar, S. S.; Tomasi, J.; Barone, V.; Mennucci, B.; Cossi, M.; Scalmani, G.; Rega, N.; Petersson, G. A.; Nakatsuji, H.; Hada, M.; Ehara, M.; Toyota, K.; Fukuda, R.; Hasegawa, J.; Ishida, M.; Nakajima, T.; Honda, Y.; Kitao, O.; Nakai, H.; Klene, M.; Li, X.; Knox, J. E.; Hratchian, H. P.; Cross, J. B.; Adamo, C.; Jaramillo, J.; Gomperts, R.; Stratmann, R. E.; Yazyev, O.; Austin, A. J.; Cammi, R.; Pomelli, C.; Ochterski, J. W.; Ayala, P. Y.; Morokuma, K.; Voth, G. A.; Salvador, P.; Dannenberg, J. J.; Zakrzewski, V. G.; Dapprich, S.; Daniels, A. D.; Strain, M. C.; Farkas, O.; Malick, D. K.; Rabuck, A. D.; Raghavachari, K.; Foresman, J. B.; Ortiz, J. V.; Cui, Q.; Baboul, A. G.; Clifford, S.; Cioslowski, J.; Stefanov, B. B.; Liu, G.; Liashenko, A.; Piskorz, P.; Komaromi, I.; Martin, R. L.; Fox, D. J.; Keith, T.; Al-Laham, M. A.; Peng, C. Y.; Nanayakkara, A.; Challacombe, M.; Gill, P. M. W.; Johnson, B.; Chen, W.; Wong, M. W.; Gonzalez, C.; Pople, J. A. *Gaussian 03*, revision B.01; Gaussian, Inc.: Pittsburgh, PA, 2003.

(37) (a) Dunning, T. H., Jr. *J. Chem. Phys.* **1989**, *90*, 1007. (b) Kendall, R. A.; Dunning, T. H., Jr.; Harrison, R. J. *J. Chem. Phys.* **1992**, *96*, 6796.

(38) Dunning, T. H., Jr.; Peterson, K. A.; Wilson, A. K. *J. Chem. Phys*. **2001**, *114*, 9244.

(39) Peterson, K. A.; Woon, D. E.; Dunning, T. H., Jr. *J. Chem. Phys*. **1994**, *100*, 7410.

(40) (a) Woon, D. E.; Dunning, T. H., Jr. *J. Chem. Phys.* **1995**, *103*, 4572. (b) Peterson, K.; Dunning, T. H., Jr. *J. Chem. Phys*. **2003**, *117*, 10548.

(41) Davidson, E. R.; Ishikawa, Y.; Malli, G. L. *Chem. Phys. Lett.* **1981**, *84*, 226.

(42) MOLPRO is a package of ab initio programs written by H.-J. Werner and P. J. Knowles, with contributions from R. D. Amos, A. Bernhardsson, A. Berning, et al.

(43) Hsu, C.-W.; Ng, C. Y. *J. Chem. Phys.* **1994**, *101*, 5596.

(44) Woo, H. K.; Wang, P.; Lau, K.-C.; Xing, X.; Ng, C. Y. *J. Chem. Phys.* **2004**, *120*, 9561.

(45) Jungen, Ch.; Pratt, S. T. *J. Chem. Phys.* **1997**, *106*, 9529.